Hybrid-Field Channel Estimation for Extremely Large Aperture Arrays

Derico Pratama
School of Science and Engineering
The Chinese University of Hong Kong, Shenzhen
Shenzhen, China
dericopratama@link.cuhk.edu.cn

***Abstract*—Extremely Large Aperture Arrays (ELAA) or XL-MIMO is a promising design for future generations of mobile communications. It contains more antenna elements and can be deployed over a wide area–enabling more ubiquitous connectivity, higher spatial resolution and higher average throughput. However, due to its large size, there are currently a few open problems associated with the channel estimation of ELAA. One problem is the near-field channel properties, where the received signal becomes spherical. This has never been addressed in previous generations of mobile communications, since their antennas are compact and the far-field planar-wave assumption holds true. In a practical environment, the small-scale fading faced by ELAA can be affected by both the far-field and near-field channel. Recently, a hybrid-field channel estimation scheme based on the orthogonal matching pursuit was proposed. However, the algorithm requires prior knowledge of the channel sparsity, which are often not available in practical situations. To solve this problem, we propose the hybrid-field sparsity adaptive matching pursuit (HF-SAMP) algorithm, which performs blind estimation when the sparsity is unknown. Simulation results show that the proposed algorithm achieves better performance with lower complexity.**

***Index Terms*—Extremely Large Aperture Array, XL-MIMO, Channel estimation, Non-stationary, Near-field, Hybrid-field, OMP, SAMP, Polar domain**

I. Introduction

Massive MIMO is a key technology in 5G that sets unprecedented spectral efficiency and allows for the implementation of a wide range of new applications in broadband communications, massive machine-type communications and ultra-reliable and low latency communications. The main difference between massive MIMO and its predecessors is in its larger number of antenna elements [1]. Using many antennas allows for better spatial multiplexing through *beamforming*, where the transmitted signal is directed towards a certain spatial direction instead of broadcasted in all directions. This increases the signal gain in the location of the targeted terminal, while also reduces mutual interference in other locations [2].

However, Massive MIMO is not exactly massive. A typical design of massive MIMO consists of 64 antennas, with a dimension of 8×8. With the advent of the internet of things (IoT), a new antenna system design is needed for future generations of mobile communications; which can incorporate much larger number of antennas and serve many devices simultaneously. In addition, Massive MIMO is typically designed as a compact array, where the antenna elements are stored in a small box with antenna separation in the order of the carrier wavelength [1]. However, the spatial resolution of an array is determined by its aperture, so it is generally beneficial to spread out the antennas [2]. To improve the current 5G systems, a new antenna paradigm with truly massive scales is needed.

Extremely Large Aperture Array (ELAA) or XL-MIMO is a design fits the requirements. By definition, ELAA or XL-MIMO is an extension of Massive MIMO with much larger number of antennas, which can be deployed over a wide area [3]. Theoretically, ELAA systems should experience improved spatial resolution as well as an increase in the number of terminals they can serve. With increased spatial resolution, the signal transmitted from the array no longer resembles a beam directed towards a certain direction. Instead, it can be viewed as strong coherent signal amplification at the exact point of the terminal's location [2]. This further reduces mutual interference in other locations in space. Due to these properties, ELAA is a great design candidate for deployments in crowded areas or in places with large volumes of IoT devices. However, there are currently a few open problems associated with ELAA systems, one of which is the *near-field propagation* properties.

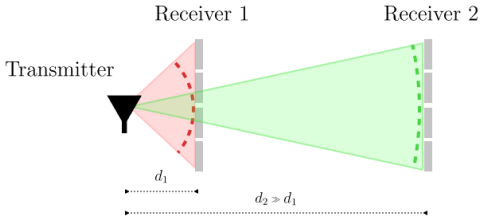

Fig. 1: Spherical wave in the near-field region vs. planar wave in the far-field region.

Electromagnetic waves can be viewed as planar or spherical, depending on where the receiver is located relative to the Rayleigh distance of the transmitter. The Rayleigh distance is given by $Z = \frac{2D^2}{\lambda}$, where D is the aperture of the array and λ is the wavelength of the carrier. When the receiver is outside the Rayleigh distance, it is said to be in the far-field region

and the signal it receives can be approximated by a planar wave. When the receiver is inside the Rayleigh distance, it is said to be in the near-field region. In the near-field region, the wave can no longer be approximated as a planar one, but must be represented as a spherical one. For current 5G Massive MIMO systems, the antenna aperture is small and the Rayleigh distance only spans several meters [4]. Moreover, 5G antennas are generally deployed on the rooftops of buildings, therefore we can safely assume that all users are located in the far-field region. For future ELAA systems, however, the aperture will be large and the Rayleigh distance spans from several hundred meters up to several kilometers wide [4]. Therefore, some users are going to be located in the near-field region. The current channel estimation methods cannot be implemented in ELAA systems, since they were designed based on the planar-wave far-field assumptions [4].

Current 5G Massive MIMO systems exploit the sparsity in the angle domain to efficiently estimate the far-field channel. This, however, does not work in ELAA systems as the angles are spread, and the channel becomes non-sparse in the angle domain due to the near-field spherical-wave effect. To address the near-field channel properties, [4] introduced the sparse polar-domain representation. The polar-domain representation includes not only the angle information but also the distance (spatial depth) information of the channel. It is proven that the near-field channel is sparse in the polar domain [4], [5]. Hence, useful channel state information can be efficiently extracted using any compressive sensing (CS) algorithm.

In real-world environment, there will be a mixture of near-field and far-field elements in ELAA systems [6]. As such, [6] proposed the hybrid-field orthogonal matching pursuit (HF-OMP) algorithm that takes into account elements from both fields. It exploits the sparsity of the channel by using the orthogonal matching pursuit (OMP) algorithm to efficiently estimate the far-field and near-field components separately in the angle and polar domain, before combining them to reconstruct the hybrid channel. However, the algorithm requires prior knowledge of the channel sparsity, which is needed to determine the number of support sets the OMP algorithm will search for during the estimation. Unfortunately, the sparsity information is rarely available in practical situations [7].

To fill in this gap, we propose a new hybrid-field channel estimation scheme based on the sparsity adaptive matching pursuit (SAMP) algorithm. Below are the contributions of this paper.

1) We reveal the limitation of HF-OMP by showing how the availability of the sparsity information can affect its performance. We also show that the channel sparsity changes as the environment changes, so it is impossible to determine its value in advance.
2) To solve the problem, we propose the hybrid-field SAMP (HF-SAMP) algorithm, which does not require any prior information on the channel sparsity. The algorithm uses SAMP to individually estimate the near-field and far-field elements in their respective sparse domains, and then combines them to reconstruct the hybrid-field channel.

Notations: Boldface uppercase and lowercase letters $\boldsymbol{a}$ and $\boldsymbol{A}$ are used to denote matrices and vectors; $(\cdot)^H, (\cdot)^\dagger, ||\cdot||$ and $|\cdot|$ denote Hermitian, Moore-Penrose pseudo-inverse matrix, Euclidean norm and the absolute value of a complex vector respectively. Finally, $\mathcal{CN}(\mu, \sigma)$ denotes the probability density function of the complex Gaussian distribution with mean μ and variance σ^2, and $\mathcal{U}(-a, a)$ denotes the probability density function of the uniform distribution on $(-a, a)$.

II. System Model

In this section, we will introduce the signal model of the ELAA system. We will also describe the far-field, near-field and hybrid-field channel models in the subsequent parts.

A. Signal Model

We consider a MISO channel where the base station (BS) employs an *N*-element ELAA system that communicates to a single-antenna user. Let $\boldsymbol{h} \in \mathbb{C}^{NX1}$ denotes the downlink channel between the BS and the user. Each of the *N* antenna elements transmits a pilot signal over *M* time slots, represented by $\boldsymbol{P} \in \mathbb{C}^{MXN}$. A complex Gaussian noise $\boldsymbol{n} \sim \mathcal{CN}(0, \sigma^2 \boldsymbol{I}_M) \in \mathbb{C}^{M\times 1}$ is also added to the received signal. The final received signal model can be described as

$$\boldsymbol{y} = \boldsymbol{P}\boldsymbol{h} + \boldsymbol{n}. \tag{1}$$

The pilot sequence $\boldsymbol{P}$ and the distribution of the noise term $\boldsymbol{n}$ are assumed to be known by the BS and the user. Therefore, the channel response $\boldsymbol{h}$ can be estimated as long as the received signal $\boldsymbol{y}$ is obtained.

B. Channel Models

We will consider the hybrid-field channel, where some scatters are located in the near-field region and the others in the far-field region [6]. To characterize this environment, we will use the hybrid-field channel model proposed by [6], which includes both the far-field and near-field terms. In the following, we will first introduce the traditional far-field channel model, and then the near-field channel model proposed by [4]. We will discuss the differences between the two models. Finally, we will introduce the hybrid-field model proposed by [6].

1) Far-Field Channel Model: Based on [4] and [8], we model the far-field channel $\boldsymbol{h}_f \in \mathbb{C}^{N\times 1}$ as

$$\boldsymbol{h}_f = \sqrt{\frac{N}{L}} \sum_{l=1}^{L} \alpha_l \boldsymbol{a}(\theta_l), \tag{2}$$

where *L* is the number of paths (scatters or users). α_l, θ_l and $\boldsymbol{a}(\theta_l)$ correspond to the gain, angle and steering vector of the *l*th path respectively. For planar waves, the steering vector is formulated as

$$\boldsymbol{a}(\theta_l) = \frac{1}{\sqrt{N}} \left[1, e^{-j\pi\theta_l}, \ldots, e^{-j(N-1)\pi\theta_l}\right]^H. \tag{3}$$

where $\theta_l \in (0, \pi)$ is normally assumed in practical cases.

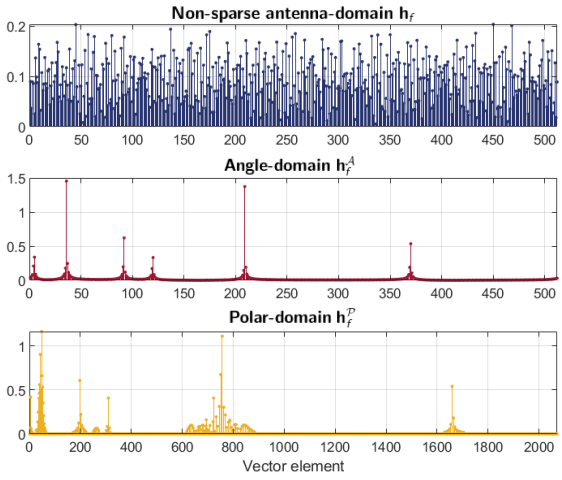

Fig. 2: The far-field channel vector in the antenna domain, angle domain and polar domain. It is sparse in the angle domain, but suffers energy leakage in the polar domain.

Based on compressive sensing (CS) techniques, we can further decompose the non-sparse $\boldsymbol{h}_f$ into a sparse representation $\boldsymbol{h}_f^{\mathcal{A}} \in \mathbb{C}^{N\times 1}$ in the angle domain. The relationship between $\boldsymbol{h}_f$ and $\boldsymbol{h}_f^{\mathcal{A}}$ is given by

$$\boldsymbol{h}_f = \boldsymbol{F}\boldsymbol{h}_f^{\mathcal{A}}. \tag{4}$$

The angle-domain transform (DFT) matrix $\boldsymbol{F} \in \mathbb{C}^{N\times N}$, which can be described as

$$\boldsymbol{F} = [\boldsymbol{a}(\theta_1), \ldots, \boldsymbol{a}(\theta_N)], \tag{5}$$

is chosen as the basis of the CS, with the sampling angles $\theta_n = \frac{2n-N-1}{N}$ for $n = 1, 2, \ldots, N$. As seen in Fig. 2, the number of non-zero elements in $\boldsymbol{h}_f^{\mathcal{A}}$ is reduced to a very small amount. In this case, the six peaks indicate the number of resolvable paths (scatters) in the channel, which is set to exactly six in the simulation. Due to the sparseness, the angle-domain representation $\boldsymbol{h}_f^{\mathcal{A}}$ can be efficiently recovered by any state-of-the-art CS algorithm.

2) Near-Field Channel Model: Based on [4], we model the near-field channel $\boldsymbol{h}_n \in \mathbb{C}^{N\times 1}$ as

$$\boldsymbol{h}_n = \sqrt{\frac{N}{L}} \sum_{l=1}^{L} \alpha_l \boldsymbol{b}(\theta_l, r_l), \tag{6}$$

where $\boldsymbol{b}(\theta_l, r_l)$ is the steering vector modeled after the spherical wave, which is formulated as

$$\boldsymbol{b}(\theta_l, r_l) = \frac{1}{\sqrt{N}} \left[1, e^{-j\frac{2\pi}{\lambda}(r_l^{(1)} - r_l)}, \ldots, e^{-j\frac{2\pi}{\lambda}(r_l^{(N)} - r_l)}\right]^H, \tag{7}$$

where r_l is the distance between the lth scatter to the center of the antenna array, and $r_l^{(n)} = \sqrt{r_l^2 + \delta_n^2 d^2 - 2r_l\delta_n d\theta_l}$ is the distance between that scatter to the nth antenna element with the coordinate $(0, \delta_n d)$. Also note that $\theta_l \in [-1, 1]$ denotes the spatial angle, $\delta_n = \frac{2n-N+1}{2}$ for $n = 0, 1, \ldots, N-1$ denotes the relative distance of the nth antenna element to the center, and $d = \frac{\lambda_c}{2}$ denotes the antenna element spacing. Comparing between (2) and (6), we see that the only difference between the far-field and near-field channel model lies in the steering vectors $\boldsymbol{a}(\theta_l)$ and $\boldsymbol{b}(\theta_l, r_l)$. While $\boldsymbol{a}(\theta_l)$ only characterizes the angles of the scatters, $\boldsymbol{b}(\theta_l, r_l)$ includes both the angle and distance information.

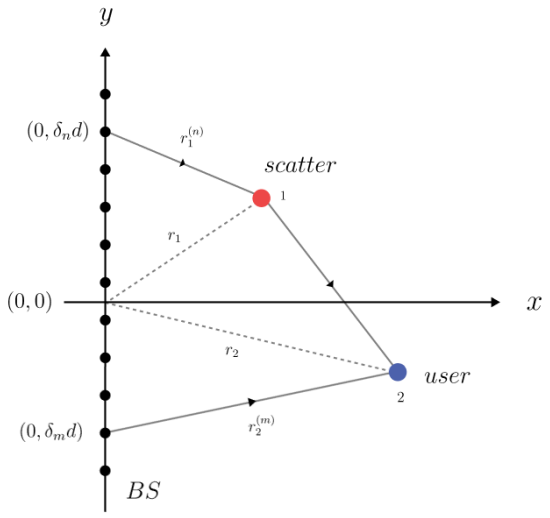

Fig. 3: The near-field channel model with LOS and NLOS path [4].

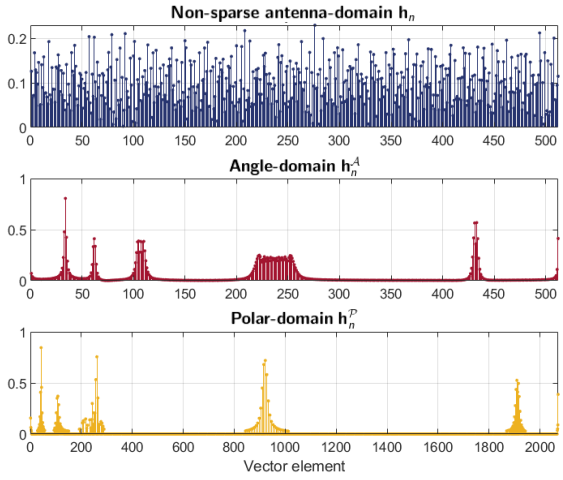

Fig. 4: The near-field channel vector in the antenna domain, polar domain and angle domain. It has better sparsity in the polar domain than in the angle domain.

As seen in Fig. 4, the near-field channel response $\boldsymbol{h}_n$ is not so sparse in the angle domain. If we estimate $\boldsymbol{h}_n$ in the angle domain using a CS-based algorithm, there will be severe performance degradation. Recently, [4] proposed the sparse polar-domain representation $\boldsymbol{h}_n^{\mathcal{P}}$ for the near-field channel.

The sparse representation is obtained by using the polar-domain transform matrix $\boldsymbol{W}$, which accounts for both the angle and distance information of the channel. The relationship between the near-field channel response and its polar-domain representation can be expressed as

$$\boldsymbol{h}_n = \boldsymbol{W}\boldsymbol{h}_n^{\mathcal{P}}, \tag{8}$$

where the polar-domain transform matrix $\boldsymbol{W}$ is formulated as

$$\begin{aligned}\boldsymbol{W} = [&\boldsymbol{b}(\theta_1, r_1^1), \ldots, \boldsymbol{b}(\theta_1, r_1^{S_1}), \ldots, \\ &\boldsymbol{b}(\theta_N, r_N^1), \ldots, \boldsymbol{b}(\theta_N, r_N^{S_N})].\end{aligned} \tag{9}$$

Each column in $\boldsymbol{W}$ represents the steering vector of the nth sampling angle θ_n and its sampling distance $r_n^{s_n}$. Note that for each θ_n, there are S_n sampling distances. Therefore, the total number of sampling distances can be calculated as $S = \sum_{n=1}^{N} S_n$. Therefore, the matrix $\boldsymbol{W}$ will have the size of $N \times S$, where $S \gg N$.

3) Hybrid-Field Channel Model: In real environments, it is very likely that the scatters are spread across both the far-field and near-field regions [6]. Based on (2) and (6), [6] proposed the hybrid channel model as

$$\boldsymbol{h}_h = \sqrt{\frac{N}{L}}\left(\sum_{l_f=1}^{\gamma L} \alpha_{l_f}\boldsymbol{a}(\theta_{l_f}) + \sum_{l_n=1}^{(1-\gamma)L} \alpha_{l_n}\boldsymbol{b}(\theta_{l_n}, r_{l_n})\right) \tag{10}$$

where L is the total number of paths (scatters) and $\gamma \in [0, 1]$ is an adjustable parameter that determines the proportion of the scatters in the far-field region. The number of paths associated with the near-field region is hence given by $(1-\gamma)L$. We see that $\boldsymbol{h}_h$ is just a generalized form of $\boldsymbol{h}_f$ and $\boldsymbol{h}_n$, since $\gamma = 1$ or $\gamma = 0$ will set it to either of the two models.

In a hybrid channel environment, using only either the angle domain or polar domain will not be sufficient to describe the channel accurately. In fact, single domain representations can cause serious performance degradation, especially in CS-based channel estimation schemes [6]. This is because the near-field response $\boldsymbol{h}_n$ is not sparse under the angle domain, as seen in Fig. 4. Likewise, the polar domain is also not suitable for the far-field response $\boldsymbol{h}_f$, since the large dimension of $\boldsymbol{W}$ can cause more energy leakage compared to the angle domain [6], which is shown in Fig. 2. Therefore, we need to separate the two channels clearly when modelling the hybrid-field environment, and then estimate them independently before combining them into a unified hybrid-field channel response in the end. Based on (1), (4) and (8), we can describe the received signal $\boldsymbol{y}$ as

$$\begin{aligned}\boldsymbol{y} &= \boldsymbol{P}\boldsymbol{h}_h + \boldsymbol{n} \\ &= \boldsymbol{P}\boldsymbol{h}_f + \boldsymbol{P}\boldsymbol{h}_n + \boldsymbol{n} \\ &= \boldsymbol{P}\boldsymbol{F}\boldsymbol{h}_{\mathcal{A}} + \boldsymbol{P}\boldsymbol{W}\boldsymbol{h}_{\mathcal{P}} + \boldsymbol{n},\end{aligned} \tag{11}$$

where $\boldsymbol{h}_f$ and $\boldsymbol{h}_n$ are the far-field and near-field components of the hybrid-field channel $\boldsymbol{h}_h$. The far-field and near-field channels are further deconmposed into their sparse representations in the angle and polar domain, respectively.

III. Channel Estimation for ELAA Systems

Looking at the terms in (11), we see that $\boldsymbol{y}$ and $\boldsymbol{P}$ are available on the receiver side. Moreover, $\boldsymbol{F}$ and $\boldsymbol{W}$ can also be sampled and calculated before the estimation using (5) and (9) respectively. Therefore, the channel estimation comes down to finding $\boldsymbol{h}_{\mathcal{P}}$ and $\boldsymbol{h}_{\mathcal{A}}$, which are sparse in the angle and polar domain respectively. Hence, CS algorithms can be used to estimate them efficiently, while the far-field and near-field channel responses can be calculated using (4) and (8) in the end.

In the following, we will introduce the existing HF-OMP [6] channel estimation algorithm for hybrid-field ELAA systems and discuss its limitations. Then, we will introduce the sparsity adaptive matching pursuit (SAMP) algorithm and discuss how it can provide improvements over OMP-based algorithms. Finally, we will propose a new SAMP-based hybrid-field channel estimation, which will be called the hybrid-field sparsity adaptive matching pursuit (HF-SAMP) algorithm.

A. Existing HF-OMP Algorithm

[6] proposed the HF-OMP algotihm to estimate the hybrid-field channel (10). In the algorithm, $\boldsymbol{h}_{\mathcal{P}}$ and $\boldsymbol{h}_{\mathcal{A}}$ are estimated separately in the polar and angle domain, both using OMP. There are three parts in the proposed HF-OMP algorithm:

1) Estimate $\boldsymbol{h}_{\mathcal{A}}$ in the angle domain using OMP.
2) Estimate $\boldsymbol{h}_{\mathcal{P}}$ in the polar-domain using OMP. In this stage, the effects of the far-field components on the channel should be removed;
3) Reconstruct $\boldsymbol{h}_f$ and $\boldsymbol{h}_n$ using (4) and (8), then finally compute the hybrid channel $\boldsymbol{h}_h$.

[6] showed that HF-OMP offers promising results in the simulations using hybrid-field channel model. However, we identified a few limitations of the HF-OMP algorithm, which are mainly related to the implementation of the OMP algorithm. In the following, we will discuss two of the limitations.

First, the OMP algorithm demands the prior knowledge of the channel sparsity K. The value of K is used to determine the number of support sets it needs to search. Hence, without the accurate knowledge of K, the OMP algorithm faces serious performance degradation. However, K is often unknown in real environments [8]. Channel sparsity can be influenced by multiple factors, for example the number of scatters at a given location and time, so it is generally difficult to obtain the channel sparsity information in advance. To illustrate how the knowledge of K affects HF-OMP, we simulate the algorithm on different number of scatter paths $L \in (10, 20, 30, 40, 50)$, against a set of sparsity assumptions. The result is shown in Fig. 5. We see that the NMSE performance of HF-OMP is not flat with respect to L. Moreover, for different L, the HF-OMP algorithm reaches optimality in different sparsity assumptions. These two observations indicate that the sparsity information is crucial for HF-OMP and that it can be influenced by non-deterministic factors.

Second, it is observed from Fig. 5 that HF-OMP does not scale well with the number of scatters L. Notice the huge

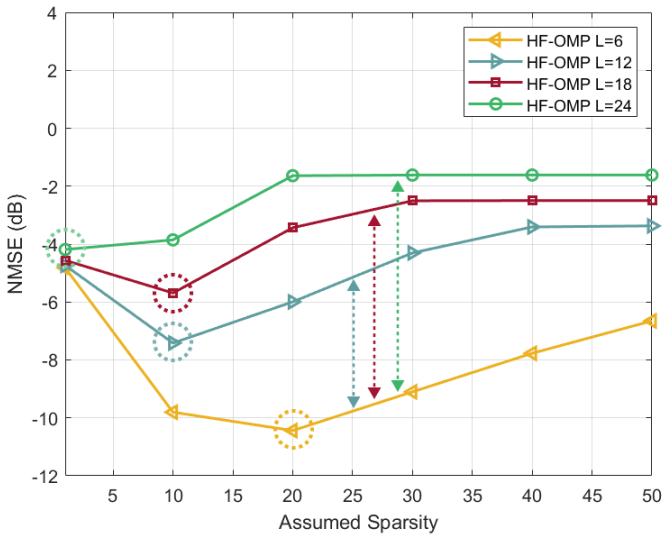

Fig. 5: NMSE performance of HF-OMP on different number of paths L against the assumed sparsity K.

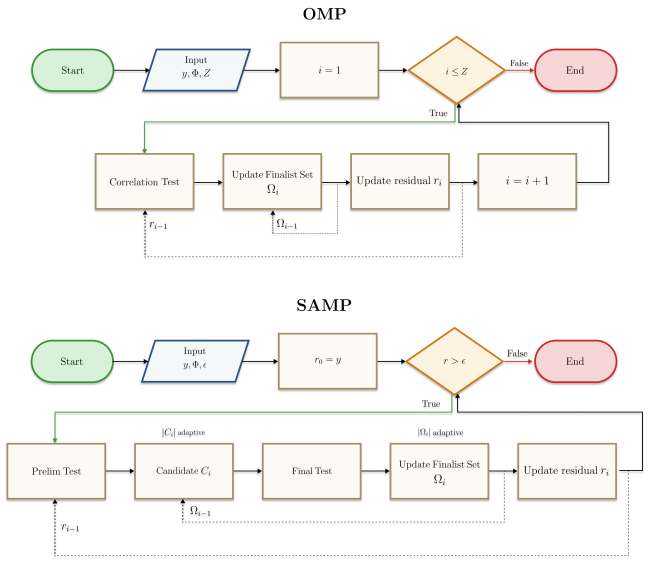

Fig. 6: Diagrams of the OMP and SAMP algorithms.

increase in the error rates as L increases. While this generally happens to all CS algorithms (since the channel becomes less sparse), several algorithms are capable of reducing this effect by approximating the actual value of the channel sparsity.

B. OMP vs. SAMP

To resolve the limitations imposed by the OMP algorithm, we introduce the sparsity adaptive matching pursuit (SAMP) algorithm [7]. As the name suggests, the SAMP algorithm does not rely on prior knowledge of the channel sparsity. Instead, the algorithm adaptively changes its support sets size to approach the true sparsity [9]. Therefore, the SAMP algorithm is expected to perform better than OMP in practical situations.

Observe the diagram in Fig. 4. The OMP algorithm is essentially a *for-loop* algorithm which stops after Z iterations, where Z is a term related to sparsity. On the other hand, the SAMP algorithm is a *while-loop* algorithm that stops after the residual term $\boldsymbol{r}$ reaches a certain threshold ϵ, which is typically set to be the noise of the channel. With OMP, there is always a possibility of underestimating or overestimating the number of iterations needed. In contrast, the number of iterations in SAMP is always precise, thereby increasing its efficiency and performance.

Finally, the implementation of SAMP allows for *backtracking*, where incorrect support sets added in previous iterations can be removed from the final set [7]. On the other hand, the selection of support sets in OMP is static–once they are included in the final set, they cannot be removed even if they are not the true support sets. Consequently, the estimated value from SAMP is always cleaner than that of the OMP.

C. Proposed HF-SAMP Algorithm

To implement the SAMP algorithm in the hybrid-field channel, the HF-SAMP algorithm is proposed. The detailed description of the proposed algorithm is given in **Algorithm 1**. Similar to HF-OMP [6], the proposed scheme is composed of three parts: 1) Near-field sparse estimation; 2) Far-field sparse estimation; and 3) Hybrid-field reconstruction. However, for Part 1 and 2, the SAMP algorithm is used instead of OMP.

The notations in **Algorithm 1** are described as follows. The variables n and f refer to the stages of the near-field and far-field iterations. $\mathcal{I}_n$ and $\mathcal{I}_f$ are the adaptive *finalist* sizes, while s is the update step-size of the *finalist* size. ρ is the SNR of the channel, and γ is the proportion of the far-field elements in the hybrid channel. Finally, the function $Max(\boldsymbol{a}, \mathcal{I})$ returns $\mathcal{I}$ indices corresponding to the largest values of the vector $\boldsymbol{a}$.

SAMP is an iterative algorithm that stops when the halting condition is met. For each of the near-field and far-field estimations, different halting conditions are implemented. As shown in Step 3 and 20, the iteration will only stop when the residual power is below a certain threshold: ϵ_n for the near-field estimation and ϵ_f for the far-field estimation. The threshold for the near-field estimation ϵ_n is set as

$$\epsilon_n = \frac{||\boldsymbol{y}||^2}{\rho + 1}(1 + \gamma\rho), \tag{12}$$

which is an approximation of the noise and the far-field power contribution. That is to say, the near-field estimation stops when there is only the far-field and noise contribution left in the residual. Similarly, the far-field estimation stops when only the contribution from the noise is left in the residual. Therefore, the far-field threshold ϵ_f is given by

$$\epsilon_f = \frac{||\boldsymbol{y}||^2}{\rho + 1}. \tag{13}$$

Algorithm 1 Hybrid-Field Sparsity Adaptive Matching Pursuit (HF-SAMP) Channel Estimation

Inputs: $\boldsymbol{y}$, $\boldsymbol{P}$, $\boldsymbol{F}$, $\boldsymbol{W}$, s, ρ, γ.
Initialize: $n = f = 1$, $\mathcal{I}_n = \mathcal{I}_f = s$, $\Omega_f = \Omega_n = \emptyset$, $\boldsymbol{r} = \boldsymbol{y}$.
// Part 1: SAMP for near-field channel in polar domain.
1. $\boldsymbol{A}_n = \boldsymbol{PW}$
2. $\epsilon_n = \dfrac{||\boldsymbol{y}||_2^2}{\rho + 1}(1 + \gamma\rho)$
3. **while** $||\boldsymbol{r}||_2^2 > \epsilon_n$
4. $S_n = Max(|\boldsymbol{A}_n^H \boldsymbol{r}|,\ \mathcal{I}_n)$ {Preliminary test}
5. $C_n = \Omega_n \bigcup S_n$ {Form candidate list}
6. $\Omega_n^{\text{new}} = Max(|\boldsymbol{A}_n{}^{\dagger}(:, C_n)\boldsymbol{y}|,\ \mathcal{I}_n)$ {Final test}
7. $\hat{\boldsymbol{h}}_{\mathcal{P}} = \boldsymbol{0}_{N\times 1}$
8. $\hat{\boldsymbol{h}}_{\mathcal{P}}(\Omega_n^{\text{new}}) = \boldsymbol{A}_n{}^{\dagger}(:, \Omega_n^{\text{new}})\boldsymbol{y}$
9. $\boldsymbol{r}^{\text{new}} = \boldsymbol{y} - \boldsymbol{A}_n\hat{\boldsymbol{h}}_{\mathcal{P}}$ {Compute residue}
10. **if** $||\boldsymbol{r}^{\text{new}}||_2 \geq ||\boldsymbol{r}||_2$ {Stage switching}
11. $n = n + 1$ {Update stage index}
12. $\mathcal{I}_n = n \times s$ {Update the size of finalist}
13. **else**
14. $\boldsymbol{r} = \boldsymbol{r}^{\text{new}}$ {Update the finalist}
15. $\Omega_n = \Omega_n^{\text{new}}$ {Update the residue}
16. **end**
// Part 2: SAMP for far-field channel in angle domain.
17. $\boldsymbol{A}_f = \boldsymbol{PF}$
18. $\epsilon_f = \dfrac{||\boldsymbol{y}||_2^2}{\rho + 1}$
19. $\boldsymbol{y} = \boldsymbol{y} - \boldsymbol{A}_n\hat{\boldsymbol{h}}_{\mathcal{P}}$
20. **while** $||\boldsymbol{r}||_2^2 > \epsilon_f$
21. $S_f = Max(|\boldsymbol{A}_f^H \boldsymbol{r}|,\ \mathcal{I}_f)$ {Preliminary test}
22. $C_f = \Omega_f \bigcup S_f$ {Form candidate list}
23. $\Omega_f^{\text{new}} = Max(|\boldsymbol{A}_f{}^{\dagger}(:, C_f)\boldsymbol{y}|,\ \mathcal{I}_f)$ {Final Test}
24. $\hat{\boldsymbol{h}}_{\mathcal{A}} = \boldsymbol{0}_{N\times 1}$
25. $\hat{\boldsymbol{h}}_{\mathcal{A}}(\Omega_f^{\text{new}}) = \boldsymbol{A}_f{}^{\dagger}(:, \Omega_f^{\text{new}})\boldsymbol{y}$
26. $\boldsymbol{r}^{\text{new}} = \boldsymbol{y} - \boldsymbol{A}_f\hat{\boldsymbol{h}}_{\mathcal{A}}$ {Compute residue}
27. **if** $||\boldsymbol{r}^{\text{new}}||_2 \geq ||\boldsymbol{r}||_2$ {Stage switching}
28. $f = f + 1$ {Update stage index}
29. $\mathcal{I}_f = f \times s$ {Update the size of finalist}
30. **else**
31. $\boldsymbol{r} = \boldsymbol{r}^{\text{new}}$ {Update the finalist}
32. $\Omega_f = \Omega_f^{\text{new}}$ {Update the residue}
33. **end**
// Part 3: Reconstruct $\hat{\boldsymbol{h}}_n$, $\hat{\boldsymbol{h}}_f$ and $\hat{\boldsymbol{h}}_h$.
34. $\hat{\boldsymbol{h}}_h = \boldsymbol{0}_{N\times 1}$
35. **if** $\Omega_f \neq \emptyset$
36. $\hat{\boldsymbol{h}}_h = \hat{\boldsymbol{h}}_h + \boldsymbol{W}\hat{\boldsymbol{h}}_{\mathcal{P}}$
37. **if** $\Omega_f \neq \emptyset$
38. $\hat{\boldsymbol{h}}_h = \hat{\boldsymbol{h}}_h + \boldsymbol{F}\hat{\boldsymbol{h}}_{\mathcal{A}}$
Output: Estimated hybrid-field channel $\hat{\boldsymbol{h}}_h$.

The algorithm is described as follows. In the first part, the near-field path components will be estimated in the polar domain using SAMP. The near-field sensing matrix is computed as $\boldsymbol{A}_n = \boldsymbol{PW}$, as shown in Step 1. Then, the threshold ϵ_n is computed in Step 2. From Step 3 to 16, the SAMP algorithm is implemented to estimate the near-field channel sparse vector $\hat{\boldsymbol{h}}_{\mathcal{P}}$. In each iteration, the *preliminary test* is performed to select a *short list* S_n of $\mathcal{I}_n$ support sets corresponding to the indices with the largest correlations between $\boldsymbol{A}_n$ and $\boldsymbol{r}$. After that, a *candidate list* C_n is created by the union of S_n and the existing *finalist* Ω_n. Based on C_n, the *final test* first solves for the least squares solution of the estimation problem, then selects $\mathcal{I}_n$ indices which have the largest magnitudes to be the new *finalist* Ω_n^{new}. Using the new *finalist* set, the temporary $\hat{\boldsymbol{h}}_{\mathcal{P}}$ can be computed using the least squares method, as shown in Step 8. Then, the new residual $\boldsymbol{r}^{\text{new}}$ is computed by removing the contribution of the current estimation of the near-field components. Note that Ω_n^{new} and $\boldsymbol{r}^{\text{new}}$ are not guaranteed acceptance in the next iteration. If $\boldsymbol{r}^{\text{new}}$ is larger than the previous residue $\boldsymbol{r}$, then they will be rejected and the algorithm moves to the next stage, increasing the *finalist* size by s. The SAMP algorithm repeats until the halting condition $||\boldsymbol{r}||^2 > \epsilon_n$ is met, and the $\hat{\boldsymbol{h}}_{\mathcal{P}}$ computed in the final iteration is accepted as the estimated near-field channel sparse vector.

In the second part, the far-field path components $\hat{\boldsymbol{h}}_{\mathcal{A}}$ will be estimated in the angle domain, also using SAMP. The far-field sensing matrix $\boldsymbol{A}_f = \boldsymbol{PF}$ is used for the estimation. The process of this part is similar to that of the first part. However, it is important that the contribution of the near-field elements be removed from the far-field estimation. Therefore, in Step 19, the near-field contribution is subtracted from $\boldsymbol{y}$. Also, the threshold ϵ_f here only contains the contribution from the noise term.

After estimating $\hat{\boldsymbol{h}}_{\mathcal{P}}$ and $\hat{\boldsymbol{h}}_{\mathcal{A}}$, we can finally obtain the estimated hybrid-field channel $\hat{\boldsymbol{h}}_h$ in Part 3 by using (11).

IV. Simulation Results

For the simulations, we compare the proposed HF-SAMP based hybrid-field channel estimation scheme with the existing HF-OMP algorithm [6]. The simulation configurations are listed in Table I.

TABLE I: Simulation Configurations

BS antennas N	512	Pilot length M	256
Carrier frequency f_c	30 GHz	Pilot elements	$\{\frac{-1}{\sqrt{M}}, \frac{1}{\sqrt{M}}\}$
Paths L	6	γ	0.5
Path gain α	$\mathcal{CN}(0, 1)$	Step size s	4
Scatter angle θ	$\mathcal{U}(-1, 1)$	Scatter distance r	$\mathcal{U}(10, 80)$ m

For benchmark comparison, we also include the least squares (LS) and the minimum mean square error (MMSE) estimation scheme. LS is an estimator that seeks to minimize the sum of the squares of the discrepancies between the observed data and the fitted data [10]. It is given by

$$\hat{\boldsymbol{h}}_{\text{LS}} = (\boldsymbol{X}^H\boldsymbol{X})^{-1}\boldsymbol{X}^H\boldsymbol{y}. \tag{14}$$

where $\boldsymbol{X} \in \mathbb{C}^{N\times N}$ is the pilot matrix. We set $\boldsymbol{X}$ as an identity matrix.

On the other hand, MMSE is an estimation method that minimizes the average error of the estimated value. MMSE estimators generally perform better than LS-based algorithms.

This is because MMSE uses the channel distribution information like the autocorrelation when estimating, while LS does not. However, this also means that MMSE has a considerably higher complexity [10]. Notice that the LS estimator is also used in matching pursuit algorithms. As such, MMSE provides an interesting contrast with the proposed HF-SAMP algorithm. For the simulation, we choose the simplest MMSE channel estimator, which is the linear MMSE. It is given by

$$\hat{\boldsymbol{h}}_{\text{MMSE}} = \boldsymbol{R}_h(\boldsymbol{X}^H\boldsymbol{X}\boldsymbol{R}_h + \sigma_z^2\boldsymbol{I})^{-1}\boldsymbol{X}^H\boldsymbol{y}, \qquad (15)$$

where $\boldsymbol{R}_h = \mathbb{E}[\boldsymbol{h}\boldsymbol{h}^H]$ is the autocorrelation matrix of the channel response $\boldsymbol{h}$. Similar to the LS estimator, the pilot matrix $\boldsymbol{X}$ here is also set as an identity matrix.

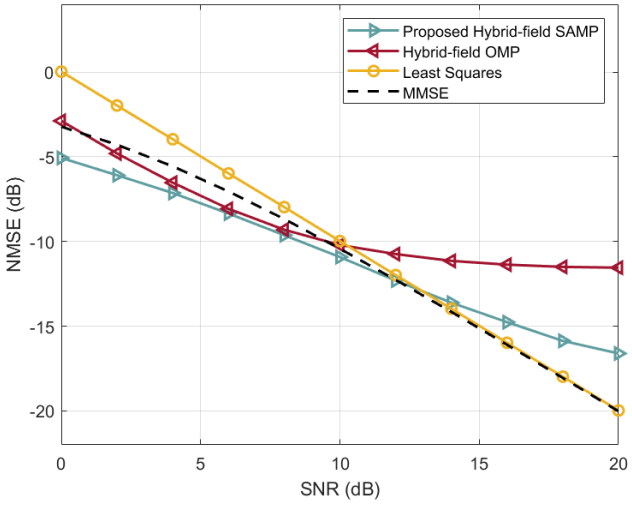

Fig. 7: NMSE performance comparison against SNR.

Fig. 7 shows the normalized mean square error (NMSE) performance comparison against the SNR from 0 dB to 20 dB. It is observed that the proposed HF-SAMP algorithm achieves better NMSE performance compared to HF-OMP at all SNR conditions. Moreover, its performance is also superior to the benchmark LS and MMSE in lower SNR up to 12 dB SNR, although it is surpassed by them in higher SNR conditions. However, it is also worth noting that both LS and MMSE have larger pilot overheads compared to HF-SAMP (512 vs. 256), so there is a trade-off between the error rate and data rate when choosing between HF-SAMP and LS or MMSE in high SNR conditions. From Table II, it can also be seen that HF-SAMP is the most efficient algorithm compared to the other three. In particular, it achieves an execution time 2.3 times faster than that of HF-OMP.

From Fig. 8, we see that both HF-OMP and the proposed HF-SAMP face performance degradation as the number of paths L increases. This is because as L increases, the sparseness of the channel decreases. However, it is also observed that the proposed HF-SAMP algorithm degrades slower than HF-OMP. This means that the proposed HF-SAMP scales better with respect to the increasing channel complexity.

TABLE II: NMSE and Execution Time of HF-OMP, HF-SAMP, LS and MMSE at SNR = 5 dB

Algorithm	NMSE (dB)	Execution time (s)
HF-OMP	-7.38	0.155
HF-SAMP	-7.84	0.066
LS	-5.06	0.078
MMSE	-6.40	0.107

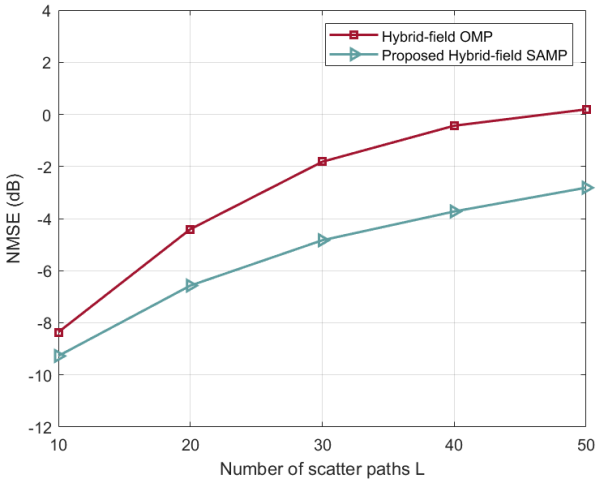

Fig. 8: NMSE performance of HF-OMP vs. HF-SAMP on different number of paths L.

Fig. 9 shows the NMSE performance comparison against different sparsity assumptions at 5 dB and 10 dB SNR. It can be observed that only HF-OMP is affected by the sparsity assumptions. At 5 dB SNR, HF-OMP performs better than LS and MMSE under ideal sparsity assumption. However, when the sparsity assumption is incorrect, it generally performs worse than MMSE, and can even be worse than the LS estimator when the sparsity is overestimated. At 10 dB SNR, HF-OMP is at best slightly better than LS and comparable to MMSE. On the other hand, the proposed HF-SAMP is always better than the other three algorithms. It is also interesting to note that even under the ideal sparsity assumption, HF-SAMP is always better than HF-OMP.

One problem faced by the SAMP algorithm is in determining the optimal step size s [7]. As seen in Fig. 10, there is a general trade-off between performance and execution time when determining s. Typically, larger s gives lower execution time, but at the cost of higher error rates. This is because the number of iterations is lower when the step size is large. Conversely, smaller s cost higher execution time, but gives lower error rates. Fortunately, there is usually an optimal s in which both the execution time and error rate is low. In the case shown in Fig. 9, the optimal s is given by $4 \leq s \leq 10$. However, such optimal s is difficult to find in advance. [9] proposed the adaptive step size SAMP (AS-SAMP) to

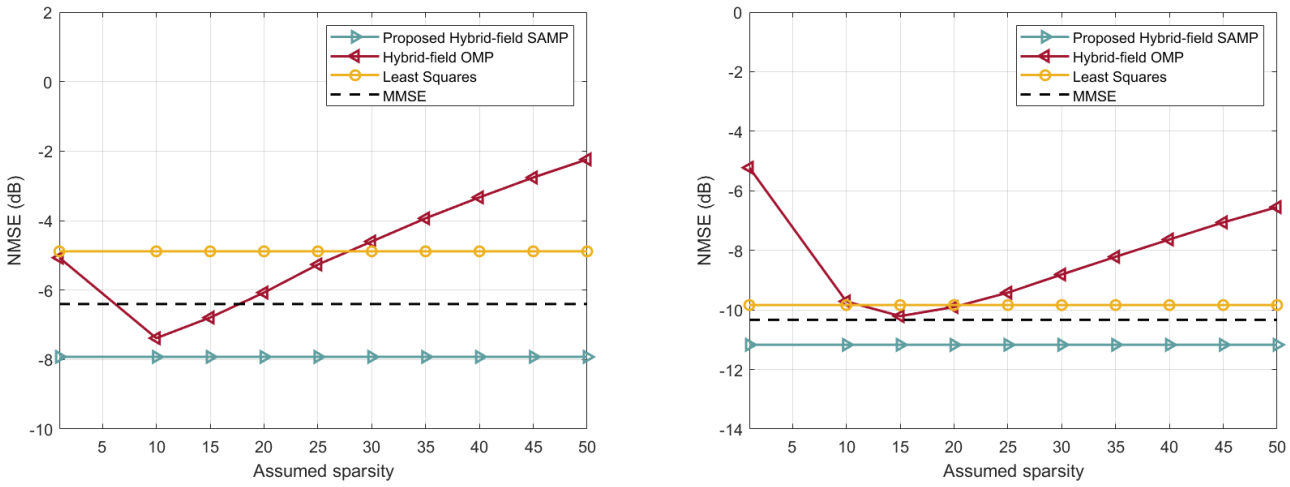

(a) SNR = 5 dB

(b) SNR = 10 dB

Fig. 9: NMSE performance comparison against sparsity assumptions at (a) 5 dB and (b) 10 dB SNR.

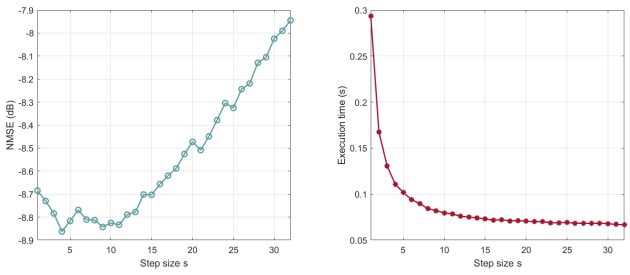

Fig. 10: Trade-off between accuracy and efficiency in determining step size s in HF-SAMP.

solve this issue. Following similar principles in SAMP, AS-SAMP adaptively changes the step size s during execution, based on some additional threshold conditions. As such, AS-SAMP can always approximate the optimal s, leading to better estimation performance. For future works, the implementation of AS-SAMP on the hybrid-field channel estimation can be considered to further improve accuracy and efficiency.

V. Conclusion

In this paper, the hybrid-field sparsity adaptive matching pursuit (HF-SAMP) algorithm is proposed to estimate the hybrid-field channel of ELAA systems. HF-SAMP improves from the existing hybrid-field channel estimation algorithm since it can operate without prior knowledge of the channel sparsity. Moreover, simulations show that it achieves better NMSE performance with lower execution time, while also having better scalability with respect to the complexity of the channel. One problem with HF-SAMP is that it is difficult to determine the step size s, which is used to adaptively change the size of the *finalist* support sets. Therefore, for future works, the adaptive step size SAMP (AS-SAMP) algorithm can be considered to further improve the accuracy and efficiency of the hybrid-field channel estimation scheme.

References

[1] E. De Carvalho, A. Ali, A. Amiri, M. Angjelichinoski and R.W. Heath, "Non-stationarities in extra-large-scale massive MIMO," *IEEE Wireless Communications*, 27(4), 2020, pp. 74-80.

[2] E. Björnson, L. Sanguinetti, H. Wymeersch, J. Hoydis, and T.L. Marzetta, "Massive MIMO is a reality—What is next?: Five promising research directions for antenna arrays," *Digital Signal Processing*, 94, 2019, pp. 3-20.

[3] Y. Han, S. Jin, C.K. Wen, and X. Ma, "Channel estimation for extremely large-scale massive MIMO systems," *IEEE Wireless Communications Letters*, 9(5), 2020, pp. 633-637.

[4] M. Cui, and L. Dai, "Channel estimation for extremely large-scale MIMO: Far-field or near-field?," arXiv preprint arXiv:2108.07581, 2022.

[5] Z. Dong, and Y. Zeng, "Near-Field Spatial Correlation for Extremely Large-Scale Array Communications," arXiv preprint arXiv:2201.03040, 2022.

[6] X. Wei, and L. Dai, "Channel Estimation for Extremely Large-Scale Massive MIMO: Far-Field, Near-Field, or Hybrid-Field?," *IEEE Communications Letters*, 26(1), 2021, pp. 177-181.

[7] T. Do, L. Gan, N. Nguyen and T. Tran, "Sparsity adaptive matching pursuit algorithm for practical compressed sensing", *2008 42nd Asilomar Conference on Signals, Systems and Computers*, 2008.

[8] H. Wang, J. Fang, P. Wang, G. Yue, and H. Li, "Efficient Beamforming Training and Channel Estimation for Millimeter Wave OFDM Systems," *IEEE Trans. Wireless Commun.*, 20(5), 2021, pp. 2805-2819.

[9] Y. Zhang, R. Venkatesan, O. A. Dobre and C. Li,"An adaptive matching pursuit algorithm for sparse channel estimation," *2015 IEEE Wireless Communications and Networking Conference (WCNC)*, 2015, pp. 626-630.

[10] M.B. Sutar and V.S. Patil, "LS and MMSE Estimation with Different Fading Channels for OFDM System," *International Conference on Electronics, Communication and Aerospace Technology (ICECA)*, 2017, pp. 740-745.